Correspondence

Area Resolution for Bistatic Ultrawideband Ultrawidebeam SAR

Conventional SAR resolution equations cannot be applied to ultrawideband ultrawidebeam systems, particularly, bistatic ultrawideband ultrawidebeam systems. This is because the dependence of system frequency response in the range and across range is not considered. In this case, area resolution, i.e., area of the resolution cell, will be an alternative. This article introduces a new area resolution formula for bistatic ultrawideband ultrawidebeam SAR systems based on the relationship between radar signal frequency, range, and cross-range wavenumbers for bistatic synthetic aperture radar.

NOMENCLATURE

List of Symbols

B	Bandwidth.
$\nu.$	Radar frequency.
ω	Angular frequency.
$\lambda.$	Wavelength.
$k.$	Wavenumber.
ϕ_0	Geometrical integration angle.
$\phi_u + \phi_l$	Bistatic integration angle.
x_0	Bistatic aperture length.
r_{TX}	Distance between transmitter and aim point.
r_{RX}	Distance between aim point and receiver.
r	Distance between aperture and aim point.
ρ_0	Minimum distance between aperture and aim point.
α_{TX}	Angle between $\vec{r}_{TX}$ and $\vec{\rho}_0$.
α_{RX}	Angle between $\vec{r}_{RX}$ and $\vec{\rho}_0$.
α	Bistatic angle.
θ_{TX}	Angle between $\vec{r}_{TX}$ and ground plane.
θ_{RX}	Angle between $\vec{r}_{RX}$ and ground plane.
θ	Angle between $\vec{r}$ and ground plane.
ζ_0	Average altitude of platforms.

I. INTRODUCTION

Resolution formulas are an important tool for designing and evaluating SAR systems. On one hand, armed with these formulas, we can regulate SAR systems parameters, such as center frequency, bandwidth, integration angle, and SAR geometry to obtain the desired resolutions. On the other hand, measuring the practical resolutions at the output of a SAR system, i.e., the SAR image, is one of the SAR

Manuscript received June 13, 2020; revised September 12, 2020; released for publication November 9, 2020. Date of publication November 24, 2020; date of current version April 10, 2021.

DOI. No. 10.1109/TAES.2020.3040067

Refereeing of this contribution was handled by S. S. Ram.

Author.s address: V. T. Vu is with the Blekinge Institute of Technology, 37179 Karlskrona, Sweden, E-mail: (viet.thuy.vu@bth.se).

image quality assessments to evaluate the performance of the SAR system by comparing them, the practical resolutions, with the theoretical resolutions given by the resolution formulas.

Bistatic SAR refers to the SAR systems with transmitter and receiver separated in space. The transmitter and receiver can be carried by different platforms or even a single platform with the antennas that are physically separated (pseudomonostatic). This spatial separation gives bistatic SAR unique advantages that have been shown in [1]. For example, the transmitter platform of a bistatic SAR system can be deployed far from an illuminated SAR scene to reduce vulnerability for military applications, whereas the receiver platform can be placed in the ground stations for simplifying data processing tasks that normally require much effort. With the multiple deployed receivers, a ground object can be observed with different bistatic angles and this helps to enhance the ability of classification. Bistatic SAR is also evaluated as a robust solution for the left/right ambiguity and the low cross-range resolution for the forward-looking SAR problem. From a system design point of view, bistatic SAR is more flexible than monostatic SAR, and thus, the cost to build a bistatic system can be optimized. Bistatic SAR is also suggested for clutter suppression when the clutter scattering is dominated by the dihedral or trihedral scattering mechanisms. To investigate the challenges of bistatic SAR, several bistatic SAR experiments have been carried out using the existing monostatic SAR systems. One of the early bistatic experiments was the hybrid bistatic SAR constellation performed in 2008 and 2009 by TerraSAR-X (spaceborne) and PAMIR (airborne) [2]. Another experiment was performed by two airborne systems LORA and SETHI in December 2009, namely, LORAMbist [3]. Recently, the experiments with ultrawideband ultrawidebeam SAR systems have been of interest. A bistatic P-band ultrawideband ultrawidebeam SAR experiment was performed in November 2015 in China [4]. The challenges with bistatic SAR, such as bistatic synchronization and bistatic processing, come from the fact that bistatic geometries are diverse because of the different velocities and different altitudes of transmitter and receiver platforms. This partly explains why the research on bistatic have been focused on synchronization and algorithm development [5]–[7]. Beside this, there have been other important research on bistatic SAR and one of them is bistatic SAR resolution.

A method to determine bistatic SAR spatial resolutions was introduced very early based on the use of the gradient [8]. Since the formulas derived from the method were given in an unclosed form, applying these formulas to design and evaluate the bistatic SAR systems was limited. In [9], this method was used to investigate Doppler and cross-range resolutions for different bistatic forward-looking SAR geometries. Several bistatic SAR spatial resolution formulas in closed form have been introduced through time, e.g., in [10] and [11]. These formulas allow the estimation of bistatic SAR spatial resolutions with bistatic SAR system parameters. However, these formulas aim at the conventional bistatic SAR systems with small fractional bandwidths (the ratio of bandwidth to center frequency $B/f_c \ll 1$) and narrow integration angles (several degrees) in which the dependency of system frequency response in the range and cross-range directions are ignored. For the systems with large fractional bandwidths and wide integration angles, these bistatic SAR spatial resolution formulas cannot be applicable. In such cases, area resolution will be an alternative because the area resolution includes the dependency of system frequency response in the range and cross-range directions.

The concept of area resolution formula was introduced in [12] for the first time after CARABAS, a monostatic ultrawideband ultrawidebeam SAR system systems had been emerged. However, the area resolution formulas derived in [12] is only for monostatic SAR. An area resolution formula for bistatic SAR is unavailable in literature and still desired.

In this article, we present an investigation on area resolution aiming at bistatic ultrawideband ultrawidebeam SAR systems. The investigation is based on an analytical function representing the region support of bistatic SAR, i.e., 2-D Fourier transform of the bistatic SAR image with a single point-like scatterer. This function shows, therefore, the relationship between the wavenumbers in slant-range and cross-range, the radar signal frequency and the bistatic geometry. The function allows the derivation of a bistatic SAR area resolution.

The rest of this article is organized as follows. The relationship between radar signal frequency, range and cross-range wavenumbers for bistatic SAR is introduced in Section II. Area resolution for bistatic SAR is investigated in Section III. An area resolution formula and its simplified forms in the special case are also derived in this section. Section IV presents the simulations to validate the derived formulas. Finally, Section V concludes this article.

II. RELATIONSHIP BETWEEN RADAR SIGNAL FREQUENCY, WAVENUMBERS AND BISTATIC SAR GEOMETRY

The relationship between radar signal frequency, slant-range and cross-range wavenumbers, and bistatic SAR geometry can be derived from the kernel of the backprojection algorithm [13] and the method of stationary phase. The nomenclature is like the one that has been used for the derivation the ground-range and cross-range resolution formulas given in [10]. Fig. 1 provides the illustration of bistatic SAR geometry in a general case where the velocities of transmitter and receiver platforms are different. The coordinates of the transmitter and receiver platforms in each aperture position determine the foci of an ellipsoid for the data backprojection (black solid-filled curve in Fig. 1). The center of ellipsoid is, therefore, the midpoint of these coordinates. A set of centers of ellipsoid will form the bistatic aperture (black circles in Fig. 1). The bistatic aperture is a base from which to define the slant-range plane $(\vec{\xi},\ \vec{\rho})$. It is important to highlight that the ground-range plane is defined by $(\vec{\xi},\ \vec{\eta})$.

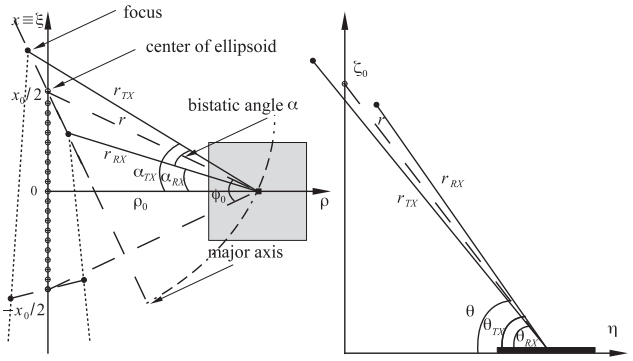

Fig. 1. Bistatic SAR geometry in a general case.

A. Derivation

According to [10], the cross-range wavenumber k_ξ is given by

$$k_\xi = \frac{2\pi\nu}{c_0}(\sin\alpha_{TX} + \sin\alpha_{RX}) \tag{1}$$

where c_0 is the speed of propagation.

To derive the relationship between radar signal frequency, wavenumbers (slant-range and cross-range) and bistatic geometry bistatic SAR, the slant-range wavenumber k_ρ is needed instead of the ground-range wavenumber k_η that has been derived in [10]. The slant-range and ground-range are linked by

$$\eta = \sqrt{\rho^2 - \zeta_0^2}. \tag{2}$$

The slant-range wavenumber is, therefore, derived by

$$k_\rho = \frac{2\pi\nu}{c_0}\frac{\partial(r_{TX} + r_{RX})}{\partial\rho} = \frac{2\pi\nu}{c_0}\frac{\partial(r_{TX} + r_{RX})}{\partial\eta}\frac{\partial\eta}{\partial\rho}. \tag{3}$$

The first part of (3) will result into the ground-range wavenumber k_η [10]

$$\begin{aligned} k_\eta &= \frac{2\pi\nu}{c_0}\frac{\partial(r_{TX} + r_{RX})}{\partial\eta} \\ &= \frac{2\pi\nu}{c_0}(\cos\alpha_{TX}\cos\theta_{TX} + \cos\alpha_{RX}\cos\theta_{RX}). \end{aligned} \tag{4}$$

The second part of (3) is derived from (2) as

$$\frac{\partial\eta}{\partial\rho} = \frac{\rho}{\sqrt{\rho^2 - \zeta_0^2}} = \frac{1}{\cos\theta}. \tag{5}$$

The final expression of the slant-range wavenumber k_ρ is shown to be

$$k_\rho = \frac{2\pi\nu}{c_0}\left(\cos\alpha_{TX}\frac{\cos\theta_{TX}}{\cos\theta} + \cos\alpha_{RX}\frac{\cos\theta_{RX}}{\cos\theta}\right). \tag{6}$$

To derive the desired relationship, we calculate the Euclidean norm of the vector $[k_\xi,\ k_\rho]$

$$\sqrt{k_\xi^2 + k_\rho^2} = \frac{2\pi\nu}{c_0}\chi \tag{7}$$

which can be rewritten

$$\omega = \frac{c_0}{\chi}\sqrt{k_\xi^2 + k_\rho^2} \tag{8}$$

where χ is so-called the bistatic factor and given by (9) shown at the bottom of this page. Equation (8) represents the relationship between radar signal frequency, wavenumbers, and bistatic SAR geometry

B. Approximations

In operational scenarios, the angles θ_{TX} and θ_{RX} are generally different and there is no approximation that can be applied to (9). But in some cases, the difference between θ_{TX} and θ_{RX} is relatively small. For example, in the bistatic experiment [2], $|\theta_{TX} - \theta_{RX}| \le 10^o$. With this knowledge, we can approximate the quotients in (9) with

$$\frac{\cos\theta_{TX}}{\cos\theta} \approx 1 \quad \text{and} \quad \frac{\cos\theta_{RX}}{\cos\theta} \approx 1. \tag{10}$$

Under such circumstances, we can simplify (9) to

$$\begin{aligned} \chi &\approx \sqrt{(\sin\alpha_{TX} + \sin\alpha_{RX})^2 + (\cos\alpha_{TX} + \cos\alpha_{RX})^2} \\ &\approx \sqrt{2 + 2\cos(\alpha_{TX} - \alpha_{RX})} \\ &\approx 2\cos\left(\frac{\alpha_{TX} - \alpha_{RX}}{2}\right) = 2\cos\frac{\alpha}{2} \end{aligned} \tag{11}$$

where α is commonly known as the bistatic angle [1]. The approximate relationship between signal frequency, wavenumbers and bistatic SAR geometry will, therefore, be written as

$$\omega \approx \frac{c_0}{2\cos(\alpha/2)}\sqrt{k_\xi^2 + k_\rho^2}. \tag{12}$$

In a more special case where the angles $\alpha_{TX} \approx \alpha_{RX}$, the bistatic angle is approximated by $\alpha \approx 0^o$. Consequently, the approximate relationship is further simplified to

$$\omega \approx \frac{c_0}{2}\sqrt{k_\xi^2 + k_\rho^2}. \tag{13}$$

Equation (13) represents the well-known relationship between signal frequency, range and cross-range wavenumbers in the monostatic case.

C. Bounds for Wavenumbers

The bounds for the wavenumbers k_ξ and k_ρ depend not only on the maximum and minimum operating frequencies but also bistatic SAR geometry, especially the initial and last SAR platform positions. These parameters decide the shape of support region of a bistatic SAR image. Fig. 2 illustrate a bistatic SAR region of support in the form of arch and marked by the hatched lines. The circular arch corresponds to a monostatic SAR region of support with the same frequency range and integration angle.

The bound for k_ξ can be retrieved based on (1) as

$$\begin{aligned} -\frac{2\pi\nu_{\max}}{c_0}\left(\sin\alpha_{T_l} + \sin\alpha_{R_l}\right) \\ \le k_\xi \le \frac{2\pi\nu_{\max}}{c_0}\left(\sin\alpha_{T_u} + \sin\alpha_{R_u}\right) \end{aligned} \tag{14}$$

where the angles $(\alpha_{T_l}, \alpha_{R_l})$ and $(\alpha_{T_u}, \alpha_{R_u})$ are the angles $(\alpha_{TX}, \alpha_{RX})$ estimated with the reference coordinates $x =$

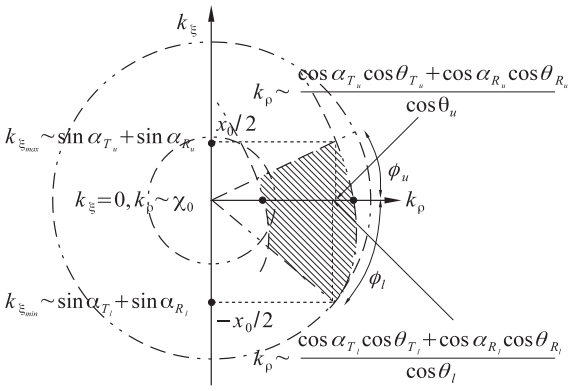

Fig. 2. Bistatic SAR region of support.

$-x_0/2$ and $x = -x_0/2$, providing the upper and lower bounds of k_ξ, respectively.

Based on (8), we can find the bound for k_ρ when $k_\xi = 0$

$$\frac{2\pi\nu_{\min}}{c_0}\chi_0 \le k_\rho \le \frac{2\pi\nu_{\max}}{c_0}\chi_0 \tag{15}$$

where χ_0 is a value of χ that corresponds to the set of angles $(\alpha_{T_0}, \alpha_{R_0}, \theta_0, \theta_{T_0}, \theta_{R_0})$, calculated for the reference coordinate $x = 0$.

D. Bistatic Integration Angle

The integration angle synthesized by a bistatic SAR system is different from the geometrical integration angle ϕ_0 that is used for the monostatic case. The bistatic integration angle can be derived from the bounds for k_ξ given by (14) and the corresponding k_ρ. As sketched in Fig. 2, the bistatic integration angle is estimated by

$$\begin{aligned}\phi_u + \phi_l = &\operatorname{atan}\left\{\frac{\cos\theta_u\left(\sin\alpha_{T_u}+\sin\alpha_{R_u}\right)}{\cos\alpha_{T_u}\cos\theta_{T_u}+\cos\alpha_{R_u}\cos\theta_{R_u}}\right\}\\ &+\operatorname{atan}\left\{\frac{\cos\theta_l\left(\sin\alpha_{T_l}+\sin\alpha_{R_l}\right)}{\cos\alpha_{T_l}\cos\theta_{T_l}+\cos\alpha_{R_l}\cos\theta_{R_l}}\right\}.\end{aligned} \tag{16}$$

In the case where the approximations given by (10) are available, the bistatic integration angle is approximated by

$$\phi_u + \phi_l \approx \frac{\alpha_{T_u}+\alpha_{R_u}}{2} + \frac{\alpha_{T_l}+\alpha_{R_l}}{2}. \tag{17}$$

The bistatic integration angle is approximated by the geometrical integration angle, i.e., monostatic integration angle when $\alpha_{T_u} - \alpha_{R_u} \approx 0$ and $\alpha_{T_l} - \alpha_{R_l} \approx 0$, i.e., $\alpha_{T_u} \approx \alpha_{R_u} \approx \phi_0/2$ and $\alpha_{T_l} \approx \alpha_{R_l} \approx \phi_0/2$.

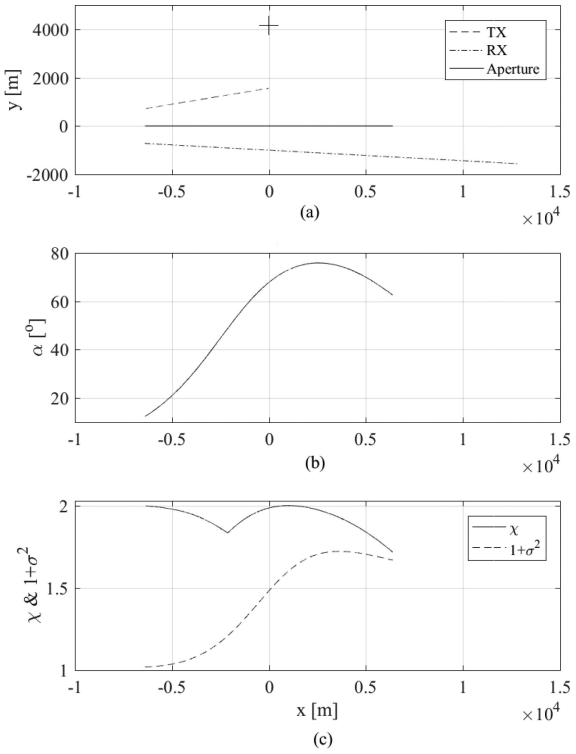

Fig. 3. Simulated bistatic geometry, bistatic angle, and corresponding factors. (a) Bistatic geometry. (b) Bistatic angle. (a) Bistatic factors.

III. AREA RESOLUTION

The concept of area resolution formula was introduced in [12] for the first time after CARABAS, a monostatic ultrawideband ultrawidebeam SAR system systems had been emerged. It was recognized that the resolution formulas that are used for conventional SAR systems do not consider the dependency of system frequency response in the range and cross-range directions. This is available for the conventional SAR systems with small fractional bandwidth and narrow integration angle so that the region of support matches approximately to a rectangle. Ultrawideband ultrawidebeam SAR systems such as CARABAS are not under such circumstances. For the bistatic cases, under the same circumstances, the region of support matches approximately to a parallelogram. Without considering the dependency of system frequency response in the range and cross-range directions, it is possible to derive the spatial resolutions formulas, as presented in [10] and [11]. However, for ultrawideband ultrawidebeam bistatic SAR systems, the dependency of system frequency response in the range and cross-range directions cannot be ignored. As observed in Fig. 2 and later in Fig. 4(b), a parallelogram is generally not optimum for bistatic ultrawideband ultrawidebeam SAR. In

$$\chi = \sqrt{(\sin\alpha_{TX}+\sin\alpha_{RX})^2 + \left(\cos\alpha_{TX}\frac{\cos\theta_{TX}}{\cos\theta} + \cos\alpha_{RX}\frac{\cos\theta_{RX}}{\cos\theta}\right)^2}. \tag{9}$$

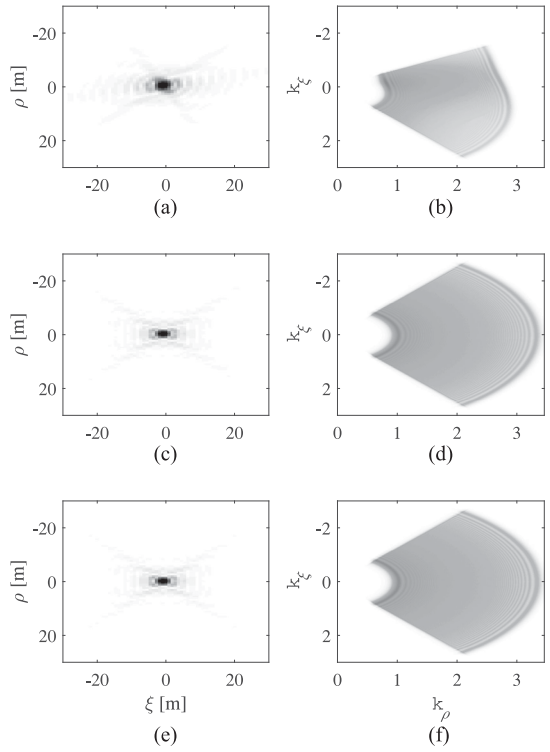

Fig. 4. Images of SAR scene and regions of support. (a) SAR image with $\alpha_{\max} = 75.9°$. (b) Region of support for (a). (c) SAR image with $\alpha_{\max} = 10.4°$. (d) Region of support for (c). (e) SAR image with $\alpha_{\max} = 0°$. (f) Region of support for (e).

this case,, area resolution should be a good replacement for these spatial resolutions formulas and used as an assessment for bistatic ultrawideband ultrawidebeam SAR systems. Using the same nomenclature presented in [12], we can derive the lower bound for the area resolution provided by a bistatic ultrawideband ultrawidebeam SAR system. Hence, the lower bound is defined by

$$\Delta A \geq \frac{(2\pi)^2}{\Omega} \tag{18}$$

where Ω is the region of support. It is given by the area of the arch

$$\begin{aligned}\Omega &= \int_{-\phi_l}^{+\phi_u} \frac{1}{2}\left[\frac{4\pi\nu_{\max}}{c_0}\chi(\phi)\right]^2 - \frac{1}{2}\left[\frac{4\pi\nu_{\min}}{c_0}\chi(\phi)\right]^2 d\phi \\ &= (2\pi)^2 \frac{1}{\lambda_c}\frac{2B}{c_0}\int_{-\phi_l}^{+\phi_u} \frac{\chi^2(\phi)}{2} d\phi \end{aligned} \tag{19}$$

where the bistatic integration angle $\phi_u + \phi_l$ is defined in (16) and different from the geometrical integration angle ϕ_0, that is limited by the beamwidth after a bistatic spatial synchronization, λ_c denotes the center wavelength of the radar signal. Since the factor χ varies with respect to ϕ, or in other words the aperture position, it is reasonable to write $\chi(\phi)$. However, it is most likely impossible to obtain an analytical expression for χ as a function of ϕ due to the fact that bistatic geometries are very complicated. With the availability of transmitter and receiver platform coordinates, the set of values of χ with respect to ϕ can be estimated. If the maximum value of the factor χ is $\chi_{\max}$, then we can apply the monotonicity property of integral to find its upper bound as

$$\begin{aligned}(2\pi)^2 \frac{1}{\lambda_c}\frac{2B}{c_0}\int_{-\phi_l}^{+\phi_u}\frac{\chi^2(\phi)}{2}d\phi &\leq (2\pi)^2 \frac{1}{\lambda_c}\frac{2B}{c_0}\int_{-\phi_l}^{+\phi_u}\frac{\chi_{\max}^2}{2}d\phi \\ &\leq (2\pi)^2 \frac{2(\phi_u+\phi_l)}{\lambda_c}\frac{2B}{c_0}\left(\frac{\chi_{\max}}{2}\right)^2. \end{aligned} \tag{20}$$

Consequently, the lower bound of bistatic SAR area resolution is derived by

$$\Delta A \geq \frac{\lambda_c}{2(\phi_u+\phi_l)}\frac{c_0}{2B}\left(\frac{\chi_{\max}}{2}\right)^{-2}. \tag{21}$$

In the less general case where the difference between θ_{TX} and θ_{RX} is relatively small, the lower bound of bistatic SAR area resolution is simplified

$$\Delta A \geq \frac{\lambda_c}{\left(\alpha_{T_u}+\alpha_{R_u}+\alpha_{T_l}+\alpha_{R_l}\right)}\frac{c_0}{2B}\left(\cos\frac{\alpha_{\min}}{2}\right)^{-2} \tag{22}$$

where $\alpha_{\min}$ is the minimum bistatic angle.

In the special case where the angles $\alpha_{TX} = \alpha_{RX}$, the bistatic angle will be $\alpha = 0°$. The lower bound of bistatic SAR area resolution is further simplified to

$$\Delta A \geq \frac{\lambda_c}{2\phi_0}\frac{c_0}{2B} \tag{23}$$

Equation (23) is identical to (7) in [12] that is the lower bound for area resolution for the monostatic case.

IV. SIMULATIONS

In this section, we provide some simulation results to show the practical issues with the spatial resolution formulas when applying to ultrawideband ultrawidebeam bistatic SAR systems. The results also validate the area resolution formula (21) proposed in the previous section. In the simulations, we use the parameters of CARABAS-II (transmitter) and CARABAS-III (receiver) to ensure that the simulated system is an ultrawideband ultrawidebeam SAR system with an extreme bistatic geometry.

A. Arrangement

The transmitter is simulated with the parameters of CARABAS-II with the fractional bandwidth $B/f_c \approx 1.2$ and 20480 aperture positions, while the passive receiver is simulated with the motion parameters of CARABAS III (speed and altitude). The main parameters for the simulations are summarized in the upper part of Table I. The speed of the receiver platform (helicopter) is 3 times lower than the one of transmitter platform (aircraft). The difference between the flight altitudes of the platforms is about 1700 m. Some supplemental parameters for the simulations are given in the lower part of table. The flight headings are $-2.5°$ the transmitter platform and $7.5°$ for the receiver transmitter platform. The flight paths are sketched in Fig. 3(a). The bistatic aperture is formed by the midpoints of the transmitter and receiver coordinates and marked by the black solid line.

TABLE I
Simulation Parameters

Parameter	Transmitter	Receiver
Maximum frequency	82.5 MHz	
Minimum frequency	22.0 MHz	
Platform speed v_{pl}	129 m/s	43 m/s
Aperture step	0.9375 m	0.3125 m
Flight altitude	3700 m	2000 m
PRF	137 Hz	
Num. aperture position	20480	
Initial coordinates	$(-6394, -721)$	$(-6369, 721)$
Last coordinates	$(12787, -1558)$	$(-24, 1558)$
Flight headings	-2.5^{o}	7.5^{o}

The ground scene is simulated with a single point-like scatterer placed in the center of the SAR scene and symmetric with respect to the bistatic aperture. It is marked by the cross in the upper part of Fig. 3(a). The radar cross-section of the scatterer is normalized to one.

With such extreme arrangement, the geometrical integration angle is about $\phi_0 \approx 103.5^{\text{o}}$ under the assumption that the antennas are omni-directional and the spatial synchronization is managed successfully. The bistatic angle is shown to be $\phi_u + \phi_l \approx 51.8^{\text{o}} + \approx 31.2^{\text{o}} = 83.1^{\text{o}}$ and significantly narrower than the geometrical integration angle. The bistatic angle varies widely with respect to the platform positions and is up to 75.9^{o} as given in Fig. 3(b). The value of bistatic factor χ estimated for each aperture position are provided in Fig. 3(c). The factor χ varies complicatedly with respect to the aperture positions and its values are in the range $[1.72,\ 2.00]$. As observed, it is very hard or even impossible to find an analytical function representing this bistatic factor.

Fig. 4(a) provides the zoomed-in section of the SAR image in the slant-range plane (ξ, ρ). The simulated point-like scatterer is well focused and the effects of both the ultrawideband ultrawidebeam and bistatic characteristics, i.e., separated sidelobe in cross-range and tilted sidelobe in slant-range, can be recognized by looking at the sidelobes of the point-like scatterer. The 2-D Fourier transform of the SAR image is given in Fig. 4(b) in the form of arch.

B. Area Resolution

1) *Exact Value:* Although the mathematical representation of $\chi(\phi)$ is unavailable to calculate the integral (19), we can still estimate the region of support by applying numerical integration to (19) thank to the available values of $\chi(\phi)$ calculated for all aperture positions. First, we apply the composite trapezoid rule with the step sizes $h = \phi_0/4$ and $2h = \phi_0/2$, and obtain $\Omega_h = (2\pi)^2 0.1884\text{m}^{-2}$ and $\Omega_{2^-h} = (2\pi)^2 0.1891\text{m}^{-2}$, respectively. Then, we apply the Richardson extrapolation on these results to get a better estimation

$$\Omega = \Omega_h + \frac{\Omega_h - \Omega_{2^-h}}{3} = (2\pi)^2\, 0.1882\text{m}^{-2} \tag{24}$$

with the truncation error is about 7×10^{-4}. The exact lower bound of the area resolution according to (18) is, therefore, $\Delta A \geq 5.3130\text{m}^2$.

2) *Conventional Spatial Resolution Formulas:* If we use the spatial resolution formulas proposed for conventional SAR systems, e.g., the ones introduced in [10], the lower bounds for cross-range and slant-range resolutions are

$$\Delta\xi = \frac{\text{c}_0\sqrt{1+\sigma^2}}{4\nu_{\max}\sin(\phi_0/2)} \geq 1.1683\text{m} \tag{25}$$

$$\Delta\rho = \frac{\text{c}_0\sqrt{1+\sigma^2}}{2B} \geq 2.4970\text{m} \tag{26}$$

where $\sigma = f/r$, i.e., the ratio of the ellipsoid's focus to its radius (see Fig. 1). The values of $1+\sigma^2$ calculated for each aperture position are provided in Fig. 3(b). The minimum value of σ is 0.1361 resulting in the minimum value of bistatic factor $\sqrt{1+\sigma^2_{\min}} = 1.0092$ and this value was used in (25) and (26). The lower bound for the area resolution is calculated by

$$\Delta A = \Delta\xi \times \Delta\rho \geq 2.9173\text{m}^2 \tag{27}$$

under the assumption that the region support of conventional SAR is a parallelogram. Comparing this value to the exact value, the relative error is about 45%.

3) *Area Resolution Formula:* The maximum value of the bistatic factor shown in Fig. 3(b) is $\chi_{\max} = 2.0006$. Equation (21) gives an estimation of area resolution lower bound as

$$\Delta A \geq \frac{\lambda_{\text{c}}}{2\,(\phi_u + \phi_l)}\frac{\text{c}_0}{2B}\left(\frac{\chi_{\max}}{2}\right)^{-2} = 4.9002\text{m}^2. \tag{28}$$

Comparing this value to the exact value, the relative error is estimated only about 8%.

C. Further Evaluation

To further evaluate the proposed area resolution formula, a simple case and a special case are considered here.

For the former, the system parameters of transmitter and receiver, and the simulated ground scene are maintained. We only change motion parameters of the platforms so that the bistatic aperture is unchanged whereas the bistatic angle increases monotonically in the range of $[0.25^{\text{o}}\ 10.4^{\text{o}}]$ and the bistatic factor χ varies in the range of $[1.9802,\ 2.0000]$. Fig. 4(c) shows the zoomed-in section of the SAR image in the slant-range plane (ξ, ρ) and the 2-D Fourier transform of the SAR image is given in Fig. 4(d) in the form of arch. The bistatic integration angle is shown to be $\phi_u + \phi_l \approx 51.7^{\text{o}} + \approx 52.4^{\text{o}} = 104.1^{\text{o}}$ that is even slightly wider than the geometrical integration angle. Applying the composite trapezoid rule with the step sizes $h = \phi_0/4$ and $2h = \phi_0/2$, and then applying the Richardson extrapolation gives us the area $\Omega = (2\pi)^2 0.2533\text{m}^{-2}$ with the truncation error is 0 (random). The exact lower bound of the area resolution is, therefore, $\Delta A \geq 3.9477\text{m}^2$. Using (10), we obtain an estimation of area resolution lower bound $\Delta A \geq 3.9142\text{m}^2$. Comparing this value to the exact value, the estimated relative error is less than 1%.

TABLE II
Exact and Estimated Area Resolution for Different Cases

Considered cases	Exact values $[\mathrm{m}^2]$	Est. values (21) $[\mathrm{m}^2]$	Relative error [%]	Est. values (25)&(26) $[\mathrm{m}^2]$	Relative error [%]
Extreme $\alpha \in [12.4^\mathrm{o}\ 75.9^\mathrm{o}]$ $\chi \in [1.72\ 2.00]$	5.3130	4.9002	7.77	2.9173	45
Simple $\alpha \in [0.25^\mathrm{o}\ 10.4^\mathrm{o}]$ $\chi \in [1.98\ 2.00]$	3.9706	3.9369	0.85	2.8642	27.9
Monostatic $\alpha = 0^\mathrm{o}$ $\chi = 2$	3.9368	3.9368	0	2.8642	27

For the later, the system parameters of transmitter and receiver, and the simulated ground scene are also maintained. We change motion parameters of the platforms so that the bistatic aperture is unchanged whereas the bistatic angle is zero, the bistatic factor is a constant $\chi = 2.00$ and $\phi_u + \phi_l = \phi_0 = 103.5^\mathrm{o}$. Hence, this special case corresponds to the monostatic case. Fig. 4(e) shows the zoomed-in section of the SAR image in the slant-range plane (ξ, ρ) and the 2-D Fourier transform of the SAR image is given in Fig. 4(f) in the form of arch. Applying the composite trapezoid rule with a step size, e.g., $h = \phi_0/2$, gives us the exact area $\Omega = (2\pi)^2 0.2540\mathrm{m}^{-2}$. The exact lower bound of the area resolution is, therefore, $\Delta A \geq 3.9368\mathrm{m}^2$. Using (21), we obtain an estimation of area resolution lower bound $\Delta A \geq 3.9368\mathrm{m}^2$ that is identical to the exact value.

All the area resolution values of the considered cases are summarized in Table II.

V. CONCLUSION

The main contribution of this article is the area resolution formula for bistatic ultrawideband ultrawidebeam SAR given by (21). The formula is given in closed form and valid for general bistatic SAR geometries. The formula was derived using the relationship between signal frequency, wavenumbers, and bistatic SAR geometry (9). The validation and evaluation for the proposed formula are performed with the several simulations. For the extreme case where the bistatic angle is up to 76°, the proposed formula had provided a good estimation of bistatic SAR area resolution with a relative error less than 8%. For the simple case with small bistatic angles, e.g., up to about 10°, the relative error caused by the proposed formula is less than 1%. The simulations also showed that it is possible to retrieve the exact value of the area resolution by using numerical integration, e.g., trapezoid rule in combination with the Richardson extrapolation.

The area resolution formula (21) facilitates bistatic resolution analysis. We can see that the area of the resolution cell depends on radar signal bandwidth, center frequency and integration angle. A higher center frequency, wider bandwidth and wider integration angle will result in better area resolution. However, the area resolution depends also on bistatic geometry that is represented by the factor χ. Although the factor χ varies complicatedly with respect to the aperture positions, under certain circumstances, this factor is shown to be proportional to the factor σ or inversely proportional to the bistatic angle α as expressed by (22).

VIET T. VU, *Senior Member, IEEE*
Blekinge Institute of Technology, Karlskrona, Sweden

REFERENCES

[1] N. J. Willis
Bistatic Radar, Boston, MA, USA: Artech House, 1991.

[2] I. Walterscheid *et al.*
Bistatic SAR experiments with PAMIR and TerraSAR-X - setup, processing, and image results
IEEE Trans. Geosci. Remote Sens., vol. 48, no. 8, pp. 3268–3279, Aug. 2010.

[3] R. Baque *et al.*
LORAMbis - A bistatic VHF/UHF SAR experiment for FOPEN in *Proc. IEEE Radar Conf.*, Washington, DC, USA, May 2010, pp. 832–837.

[4] D. An, L. Chen, H. Xiaotao, Z. Zhou, D. Feng, and T. Jin
Bistatic P-band UWB SAR experiment and raw data processing in *Proc. IEEE CIE Int. Conf. Radar*, Guangzhou, China, Oct. 2016, pp. 1–4.

[5] B. D. Rigling and R. L. Moses
Polar format algorithm for bistatic SAR
IEEE Trans. Aerosp. Electron. Syst., vol. 40, no. 4, pp. 1147–1159, Oct. 2004.

[6] Y. L. Neo, F. H. Wong, and I. G. Cumming
A two-dimensional spectrum for bistatic SAR processing using series reversion
IEEE Geosci. Remote Sens. Lett., vol. 4, no. 1, pp. 93–96, Jan. 2007.

[7] P. Lopez-Dekker, J. J. Mallorqui, P. Serra-Morales, and J. Sanz-Marcos
Phase synchronization and Doppler centroid estimation in fixed receiver bistatic SAR systems
IEEE Trans. Geosci. Remote Sens., vol. 46, no. 11, pp. 3459–3471, Nov. 2008.

[8] G. P. Cardillo
On the use of the gradient to determine bistatic SAR resolution in *Proc. IEEE Antennas Propag. Soc. Int. Symp.*, Dallas, TX, USA, May 1990, pp. 1032–1035.

[9] V. T. Vu and M. I. Pettersson
Doppler and cross-range resolutions in bistatic forward-looking SAR imaging
in *Proc. IEEE Radar Conf.*, Arlington, VA, USA, May 2015, pp. 72–76.

[10] V. T. Vu and M. I. Pettersson
Derivation of bistatic SAR resolution equations based on back-projection
IEEE Geosci. Remote Sens. Lett., vol. 15, no. 5, pp. 694–698, May 2018.

[11] W. Dower and M. Yeary
Bistatic SAR: Forecasting spatial resolution
IEEE Trans. Aerosp. Electron. Syst., vol. 55, no. 4, pp. 1584–1595, Aug. 2019.

[12] L. M. H. Ulander and H. Hellsten
A new formula for SAR spatial resolution
AEÜ Int. J. Electron. Commun., vol. 50, no. 2, pp. 117–121, 1996.

[13] L. E. Andersson
On the determination of a function from spherical averages
SIAM J. Math. Anal., vol. 19, no. 1, pp. 214–232, 1988.